($r = 0.91$) was markedly smaller than those for the remaining channels (0.98–1.00). The poor fitting suggests that this simple theoretical fitting was not available for G230A. Thus, a fitting was made assuming two independent binding sites (Fig. 4D, broken curve). A curve could be fitted with the data when assuming that 75% of the current response is mediated through a binding site having the same EC_{50} and Hill coefficient as the wild-type channel does, and the remaining 25% is mediated through another binding site having the same Hill coefficient but a larger EC_{50} value (800 μM).

3.3. ATP responsiveness and amino acid positions

In Fig. 4, we used the mean values for the curve fittings. Similar curve fittings were applied to data obtained from individual oocytes, and sensitivities to ATP were determined. pD_2 values obtained in this manner as well as the maximal current responses were plotted for the wild-type and the mutant channels in Fig. 5. For the channels with which the current responses to ATP were observed, a clear correlation was found between the maximal current amplitude and the ATP sensitivity; the channels having exhibited smaller maximal current amplitude exhibited lower sensitivity to ATP. In the amino acid sequence beginning from Ile^{226} to Gly^{230}, the substitution of an amino acid residue at an odd number position resulted in larger changes than that at an even number position. For example, the substitution of Phe^{227} resulted in the loss of ATP responsiveness, whereas the substitution of Ile^{226} or Arg^{228} did not lose the responsiveness in most cases. Similarly, the substitution of Leu^{229} resulted in large decreases in both the maximal amplitude and the ATP sensitivity, but the substitution of Arg^{228} or Gly^{230} resulted in relatively small decreases in these indexes. Within the odd or even number positions, the substitution of an amino acid residue closer to the disulfide bond involving Cys^{224} resulted in larger changes in the ATP responsiveness. The substitutions of Phe^{227} resulted in the loss of the

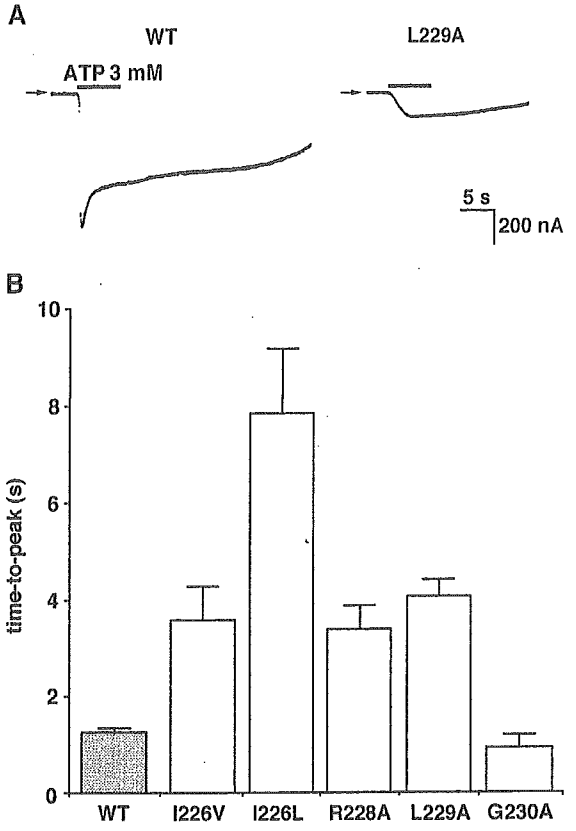

Fig. 6. Activation time course of ATP-evoked current through the wild-type and mutant channels. (A) Currents activated by 3 mM ATP in oocytes expressing the wild-type (WT) and L229A mutant channels. The oocytes were held at − 50 mV. Arrows indicate zero current levels. (B) Comparison of time required for peak current evoked by 3 mM ATP ("time-to-peak"). Each column and bar represent mean and S.E. obtained from five to eight oocytes.

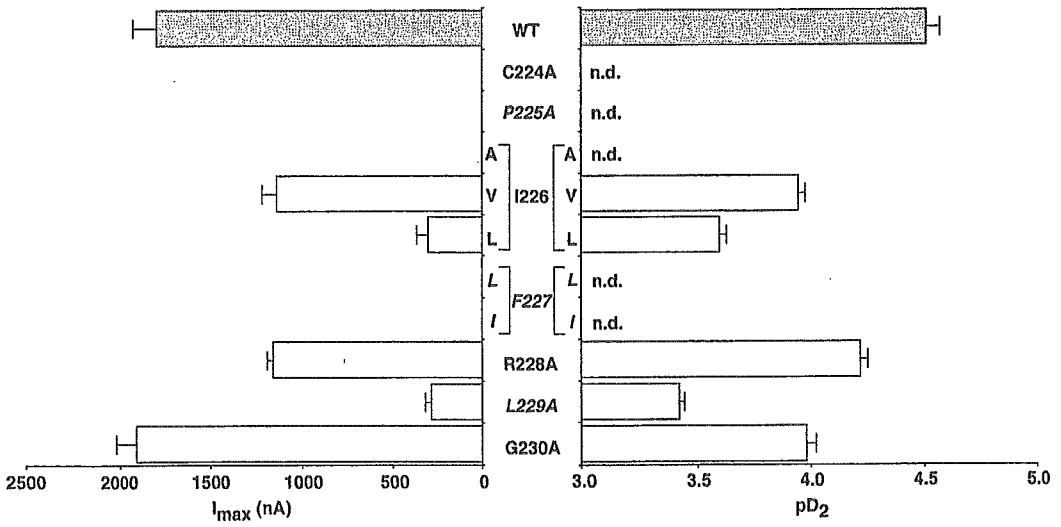

Fig. 5. Comparison of the maximal current amplitude (I_{max}) and the sensitivity to ATP (pD_2) among the wild-type and the mutant channels. The parameters were calculated from each oocytes and mean values were shown for each channel type. Bars are S.E. n.d.: not determined because of the loss of the ATP responsiveness.

responsiveness, whereas the substitution of Leu^{229} resulted in large decreases in the indexes for the responsiveness, but not in the loss of responsiveness. As for the amino acid substitutions at the even number positions, the order of the maximal current responses was Gly^{230}>Arg^{228}>Ile^{226} though the ATP sensitivities were comparable between Arg^{228} and Gly^{230}.

3.4. Activation kinetics

When ATP was applied, activation kinetics was generally faster for the wild-type channel than that for the low responsiveness mutants such as I226V or L229A. To compare the activation kinetics quantitatively, we measured the time required for peak current amplitude when activated by 3 mM ATP ("time-to-peak"; Fig. 6). The time-to-peak was <2 s for the wild-type channel, whereas it was >3 s for the low responsiveness mutants (I226V, I226L, R228A and L229A). The time-to-peak for G230V was similar to that for the wild-type channel.

4. Discussion

We have examined the effects of amino acid substitutions downward from Cys^{224} in the extracellular loop of $P2X_2$ receptor. When Cys^{224} was replaced with alanine, the responsiveness to ATP was lost (Fig. 2A), suggesting that the disulfide bond involving this residue is indispensable for the responsiveness as has been reported by Clyne et al. (2002). The alanine-substitution of Pro^{225} also resulted in the loss of the ATP responsiveness (Fig. 2A). Proline residues are able to disturb the formation of rigid structures such as α-helixes or β-sheets. This ability of Pro^{225} may provide distortion necessary for Cys^{224} to contribute to the formation of the disulfide bond.

As for the substitutions of Ile^{226}, the current response to ATP largely remained when substituted with valine (Fig. 2B,C). In contrast, the substitution with leucine resulted in a marked decrease in the current response (Fig. 2B,C). These results are puzzling because, among hydrophobic residues, leucine is similar to isoleucine in size but valine is smaller than these residues (Chothia, 1975). Interestingly, five of seven P2X receptor subclasses possess an isoleucine residue in this position, and the remaining two subclasses possess a valine residue (Fig. 1). Some common property between isoleucine and valine is necessary to maintain structures proper for the channel activation.

The substitutions of Phe^{227} with hydrophobic amino acid residues (leucine and isoleucine) resulted in the loss of the ATP responsiveness (Fig. 2A). Among P2X receptor subclasses, $P2X_3$ alone has leucine and all the remaining six subclasses have phenylalanine in this position. When Phe^{227} is replaced with leucine, five sequential amino acid residues beginning from Cys^{224} in $P2X_2$ receptor (cysteine–proline–isoleucine–leucine–arginine) completely accord with the residues at corresponding positions in $P2X_3$ receptors (Fig. 1). In spite of this fact, the replacement resulted in the loss of the channel function.

The results obtained from the alanine-substitution of Arg^{228}, Leu^{229} and Gly^{230} showed that a distinct reduction in the ATP responsiveness was found for L229A, but not for R228A or G230A (Fig. 3C). By combining these results and the results obtained from the substitutions of Ile^{226} and Phe^{227}, it appears that the replacement of the residues at odd number positions more dramatically reduces the ATP responsiveness than that at even number positions (Fig. 5). Freist et al. (1998) have pointed out that a sequence stretch of the positions 170–330 in the extracellular loop of P2X receptor proteins exhibits similarities with the catalytic domains of class II aminoacyl-tRNA synthetases as shown by secondary structure predictions and sequence alignments. In their prediction, the region involving the above-mentioned amino acid residues participates in the formation of β-sheets. If these residues are involved in the β-sheets, the residues aligning in one side (Phe^{227} and Leu^{229}) may be more influential on the channel function of P2X receptor than those in the other side (Ile^{226}, Arg^{228} and Gly^{230}).

The Hill coefficient of the wild-type $P2X_2$ receptor was about 2 (Fig. 4), which is in common with those in other reports (e.g., Nakazawa et al., 1991; Nakazawa, 1994). The value of 2 may indicate that the channel activation requires two ATP molecules (Tallarida and Jacob, 1979) though Bean (1990) has shown that the activation requires three ATP molecules at lower concentrations. The Hill coefficient of about 2 was not affected by the substitutions of the amino acid residues tested except for the alanine-substitution of Gly^{230} (Fig. 4). G230A exhibited a Hill coefficient of 1.3 when assuming homogenous binding sites (Fig. 4D, solid curve), but a better fitting could be obtained when the second binding sites of a lower affinity (Fig. 4D, broken curve). For the latter fitting, a Hill coefficient of about 2 was adopted for both the higher and the lower affinity sites. Thus, the introduction of alanine into the position 230 may not affect the number of ATP molecules for the channel activation, but may affect some process involved in the channel activation.

The present study and our previous studies (Nakazawa and Ohno, 1999; Nakazawa et al., 2002) have shown that small changes in a sequence from about the position 220 to about the position 260 in the extracellular loop can result in the loss of the ATP responsiveness. Jiang et al. (2000) also reported that alanine-substitution of Asn^{202} or Asp^{261} resulted in the loss of the ATP responsiveness. In addition, Buell et al. (1996) reported that $P2X_4$ receptor, which is insensitive to two-subclass selective purinoceptor antagonists (pyridoxal-5-phosphate-6-azophenyl-2′,4′-disulfonic acid and pyridoxal 5-phosphate), restored sensitivities to these antagonists when Glu^{249} was replaced with lysine. These results suggest that this extracellular amino acid sequence may directly contribute to some indispensable process between the recognition of ATP molecules and the

channel opening. Ennion et al. (2000) suggested that basic amino acid residues close to the channel pore (Lys^{68}, Lys^{70}, Arg^{292} and Arg^{309}) serve to recognize ATP molecules in $P2X_1$ receptor and, thus, the ATP binding pocket may form close to the outer mouth of the channel pore. Similar results were also obtained for $P2X_2$ receptor (Jiang et al., 2000). The extracellular amino acid sequence described above (the positions 224–230) is not located between this possible binding pocket and the channel pore. If this sequence contributes to some indispensable process between the recognition of ATP molecules and the channel opening, it is desired that the sequence is spatially positioned close to the "activation" link between the binding pocket and the channel pore. This view may be supported by the slower activation process observed in the low responsiveness mutants (Fig. 6). It is possible that the extracellular loop is "packed" densely enough for the sequence to reach the "activation" link.

Acknowledgements

This work was partly supported by Health and Labour Science Research Grants for Research on Advanced Medical Technology from the Ministry of Health, Labour and Welfare, Japan, and a grant-in-aid for scientific research from the Ministry of Education, Science, Sports and Culture, Japan (KAKENHI 13672319) awarded to K.N.

References

Bean, B.P., 1990. ATP-activated channels in rat and bullfrog sensory neurons: concentration dependence and kinetics. J. Neurosci. 10, 1–10.

Brake, A.J., Wagenbach, M.J., Julius, D., 1994. New structural motif for ligand-gated ion channels defined by an ionotropic ATP receptor. Nature 371, 519–523.

Buell, G., Lewis, C., Collo, G., North, R.A., Surprenant, A., 1996. An antagonist-insensitive P2X receptor expressed in epithelia and brain. EMBO J. 15, 55–62.

Chothia, C., 1975. Structural invariants in protein folding. Nature 254, 304–308.

Clyne, J.D., Wang, L.-F., Hume, R.I., 2002. Mutational analysis of the conserved cysteines of the rat $P2X_2$ purinoceptor. J. Neurosci. 22, 3873–3880.

Ennion, S.J., Evans, R.J., 2002. Conserved cysteine residues in the extracellular loop of the human $P2X_1$ receptor form disulfide bonds and are involved in receptor trafficking to the cell surface. Mol. Pharmacol. 61, 303–311.

Ennion, S., Hagan, S., Evans, R.J., 2000. The role of positively charged amino acids in ATP recognition by human $P2X_1$ receptors. J. Biol. Chem. 275, 29361–29367.

Freist, W., Verhey, J.F., Stühmer, W., Gauss, D.H., 1998. ATP binding site of P2X channel proteins: structural similarities with class II aminoacyl-tRNA synthetases. FEBS Lett. 434, 61–65.

Jiang, L.H., Rassendren, F., Surprenant, A., North, R.A., 2000. Identification of amino acid residues contributing to the ATP-binding site of a purinergic P2X receptor. J. Biol. Chem. 275, 34190–34196.

Khakh, B.S., 2001. Molecular physiology of P2X receptors and ATP signalling at synapses. Nat. Rev. 2, 165–174.

Nakazawa, K., 1994. ATP-activated current and its interaction with acetylcholine-activated current in rat sympathetic neurons. J. Neurosci. 14, 740–750.

Nakazawa, K., Ohno, Y., 1999. Neighboring glycine residues are essential for $P2X_2$ receptor/channel function. Eur. J. Pharmacol. 370, R5–R6.

Nakazawa, K., Fujimori, K., Takanaka, A., Inoue, K., 1991. Comparison of adenosine triphosphate- and nicotine-activated inward currents in rat phaeochromocytoma cells. J. Physiol. 434, 647–660.

Nakazawa, K., Ohno, Y., Inoue, K., 1998. An aspartic acid residue near the second transmembrane segment of ATP receptor/channel regulates agonist sensitivity. Biochem. Biophys. Res. Commun. 244, 599–603.

Nakazawa, K., Ojima, H., Ohno, Y., 2002. A highly conserved tryptophane residue indispensable for cloned rat neuronal P2X receptor activation. Neurosci. Lett. 324, 141–144.

Newbolt, A., Stoop, R., Virginio, C., Surprenant, A., North, R.A., Buell, G., Rassendren, F., 1998. Membrane topology of an ATP-gated ion channel (P2X receptor). J. Biol. Chem. 12, 15177–15182.

North, R.A., 2002. Molecular physiology of P2X receptors. Physiol. Rev. 82, 1013–1067.

Soto, F., Garcia-Guzman, M., Stühmer, W., 1997. Cloned ligand-gated channels activated by extracellular ATP (P2X receptors). J. Membr. Biol. 160, 91–100.

Tallarida, R.J., Jacob, L.S., 1979. The Dose–Response Relation in Pharmacology. Springer-Verlag, New York, NY.

Available online at www.sciencedirect.com

SCIENCE DIRECT®

European Journal of Pharmacology 508 (2005) 23–30

ELSEVIER

ejp

www.elsevier.com/locate/ejphar

Characterization of voltage-dependent gating of $P2X_2$ receptor/channel

Ken Nakazawa[a,*], Yasuo Ohno[b]

[a]*Cellular and Molecular Pharmacology Section, Division of Pharmacology, National Institute of Health Sciences, 1-18-1 Kamiyoga, Setagaya, Tokyo 158-8501, Japan*

[b]*Division of Pharmacology, National Institute of Health Sciences, 1-18-1 Kamiyoga, Setagaya, Tokyo 158-8501, Japan*

Received 9 September 2004; received in revised form 29 November 2004; accepted 6 December 2004
Available online 4 January 2005

Abstract

The role of a voltage-dependent gate of recombinant $P2X_2$ receptor/channel was investigated in *Xenopus* oocytes. When a voltage step to −110 mV was applied from a holding potential of −50 mV, a gradual increase was observed in current evoked by 30 μM ATP. Contribution of this voltage-dependent component to total ATP-evoked current was greater when the current was evoked by lower concentrations of ATP. The voltage-dependent gate closed upon depolarization, and half the gates were closed at −80 mV. On the other hand, a potential at which half the gates opened was about −30 mV or more positive, which was determined using a series of hyperpolarization steps. The results of the present study suggest that the voltage-dependent gate behavior of $P2X_2$ receptor is not due to simple activation and deactivation of a single gate, but rather due to transition from a low to a high ATP affinity state.

Keywords: P2X receptor; Voltage dependence; Gate; Kinetics; Ligand affinity

1. Introduction

Extracellular ATP is considered a neurotransmitter, and its fast neurotransmission is mediated through ion channel-forming P2X receptors (see reviews, Ralevic and Burnstock, 1998; Khakh, 2001; North, 2002). To date, at least seven subclasses of P2X receptor ($P2X_{1-7}$) have been cloned, which form homo- or heteromeric receptors that act as functional ion channels (North and Surprenant, 2000). Each subclass consists of two transmembrane domains (TM1 and TM2) and one long extracellular domain (E1) between them. Both TM1 (Jiang et al., 2001; Haines et al., 2001) and TM2 (Rassendren et al., 1997; Egan et al., 1998; Migita et al., 2001) contribute to formation of the channel pore. P2X receptor/channels are permeable to cations, but demonstrate poor cation selectivity. The channels are gated by ATP molecules, and the narrowest part of the channel pore opens when activated (Rassendren et al., 1997). The ATP-binding site for gating is partly attributable to basic amino acid residues near the outer mouth of the channel pore formed by TM1 and TM2 (Ennion et al., 2000; Jiang et al., 2000), and the possibility that aromatic residues in E1 contribute to the binding site has also been suggested (Nakazawa et al., 2002; Roberts and Evans, 2004).

In addition to ATP, other factors are known to modulate channel activity. Zn^{2+} and acidic conditions facilitate ATP-mediated gating by increasing ATP sensitivity of $P2X_2$ receptor (Clyne et al., 2002). Neurotransmitters, including dopamine, and related compounds also facilitate ATP-mediated gating (Nakazawa et al., 1997a). Membrane potential may also play a role. It has been reported that ionic current activated by ATP is enhanced by hyperpolarization in pheochromocytoma PC12 cells (Nakazawa et al., 1997b). We observed similar voltage-dependent gating of recombinant $P2X_2$ receptor/channel, which was originally cloned from PC12 cells (Brake et al., 1994), and qualitatively analyzed its properties in the present study.

2. Methods

Recordings of ionic current through recombinant $P2X_2$ receptor/channels were performed according to our previous

* Corresponding author. Tel.: +81 3 3700 9704; fax: +81 3 3707 6950.
E-mail address: nakazawa@nihs.go.jp (K. Nakazawa).

0014-2999/$ - see front matter © 2004 Elsevier B.V. All rights reserved.
doi:10.1016/j.ejphar.2004.12.005

report (Nakazawa and Ohno, 1997). Briefly, the cloned rat $P2X_2$ receptor (Brake et al., 1994) was expressed in *Xenopus* oocytes by injecting in vitro transcribed cRNA. After 4 days of incubation at 18 °C, the membrane current of the oocytes was recorded. Oocytes were bathed in ND96 solution containing (in mM) NaCl 96, KCl 2, $CaCl_2$ 1.8, $MgCl_2$ 1, HEPES 5 (pH 7.5 with NaOH). In some experiments, oocytes were bathed in solution containing 10.8 mM $BaCl_2$ instead of 1.8 mM $CaCl_2$. When achieving a low extracellular chloride concentration, 96 mM Na-acetate was added instead of 96 mM NaCl. ATP (adenosine 5′-triphosphate disodium salt; Sigma, St. Louis, MO, U.S.A.) was applied by superfusion for approximately 10 s at regular 2-min intervals. Membrane current was recorded using the standard two-electrode voltage-clamp techniques, and electrical signals were stored on a data recorder (PC204Ax; SONY, Tokyo, Japan) for off-line analysis. Curve fittings to data were made using Microsoft' Excel X.

3. Results

3.1. Voltage-dependent component of ATP-evoked current

Fig. 1A compares membrane currents in the absence and presence of 30 μM ATP in a $P2X_2$ receptor-expressing oocyte. The oocyte was held at −50 mV and stepped to −110 mV for 200 ms. In the presence of ATP, inward current at −110 mV did not instantaneously reach steady-state, but gradually increased: a biphasic increase in current was observed with a voltage-independent component ("a" in Fig. 1A) and a voltage-dependent component ("b" in Fig. 1A). When the voltage was returned to −50 mV, a gradually declining inward "tail" current was observed ("c" in Fig. 1A). The voltage-dependent component of the inward current at −110 mV was observed to follow first-order kinetics with a time constant of 40 ms (Fig. 1B).

Fig. 2A demonstrates an increased magnitude of the voltage-dependent component when activated from a less negative holding potential. The voltage-dependent component was larger when the step to −110 mV was applied from −10 mV ("a" in Fig. 2A) than when it was applied from −70 mV ("b" in Fig. 2A). This dependence of the voltage-dependent component on holding potentials is illustrated in Fig. 2B. It is worth noting that Ca^{2+}-activated currents exist in *Xenopus* oocytes (Weber, 1999; Zhang and Hamill, 2000). Since P2X receptor/channels are Ca^{2+}-permeable (Khakh, 2001), a secondarily activated Ca^{2+}-induced current might contribute to the observed voltage-dependent changes. This does not, however, appear to be the case since a similar dependence on holding potentials was observed when extracellular Ca^{2+} was replaced with 10.8 mM Ba^{2+}. Time constants for the activation of the voltage-dependent component were obtained as shown in Fig. 1B, and the mean values were plotted against holding potentials

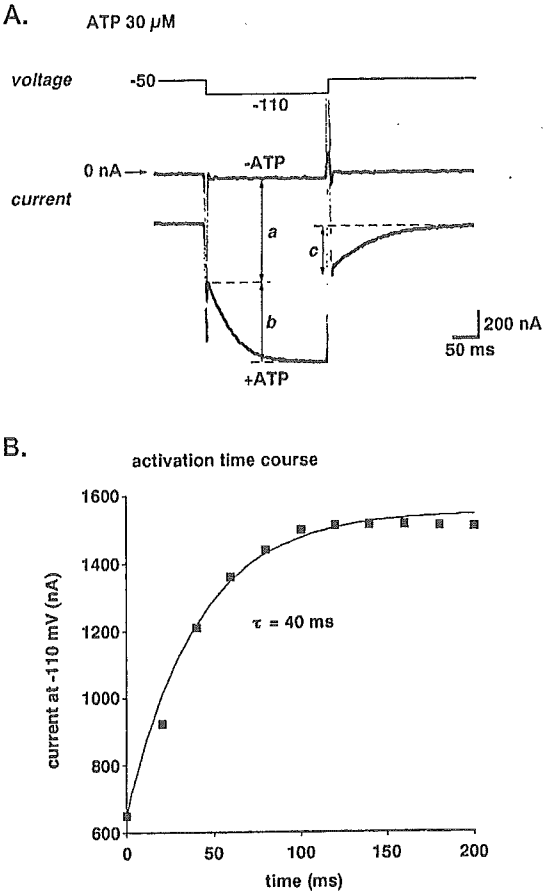

Fig. 1. (A) Current traces of an oocyte stepped to −110 mV from a holding potential of −50 mV in the absence (−ATP) or presence (+ATP) of 30 μM ATP. The current evoked by ATP is represented by the difference between the two traces. Upon hyperpolarization, a gradual increase in current was observed in the presence of ATP, suggesting activation of a voltage-dependent gate (denoted by "b"). The current denoted by "c" represents a gradually declining "tail current" that was observed when the voltage was returned to −50 mV. (B) Time course of activation of the voltage-dependent component. Current amplitude of the voltage-dependent component represented by "b" in panel A was plotted against time after the onset of hyperpolarization at −110 mV. The voltage-dependent component could be made to fit a curve with a time constant of 40 ms.

(Fig. 2C). While the current amplitude demonstrated voltage dependence (Fig. 2B), voltage did not have an effect on time course of the activation.

3.2. Effect of ATP concentrations

Fig. 3A shows the voltage-dependent component of the current activated by 10 μM or 300 μM of ATP in a single oocyte. The relative size of the voltage-dependent component involved in total ATP-evoked current became smaller when the current was evoked by greater concentrations of ATP (Fig. 3A and B). A similar dependence on ATP concentration was observed for the current evoked in the presence of 10.8 mM Ba^{2+} instead of 1.8 mM Ca^{2+} (Fig. 3B). Dependence on ATP concentrations was also found for activation time constants for the voltage-

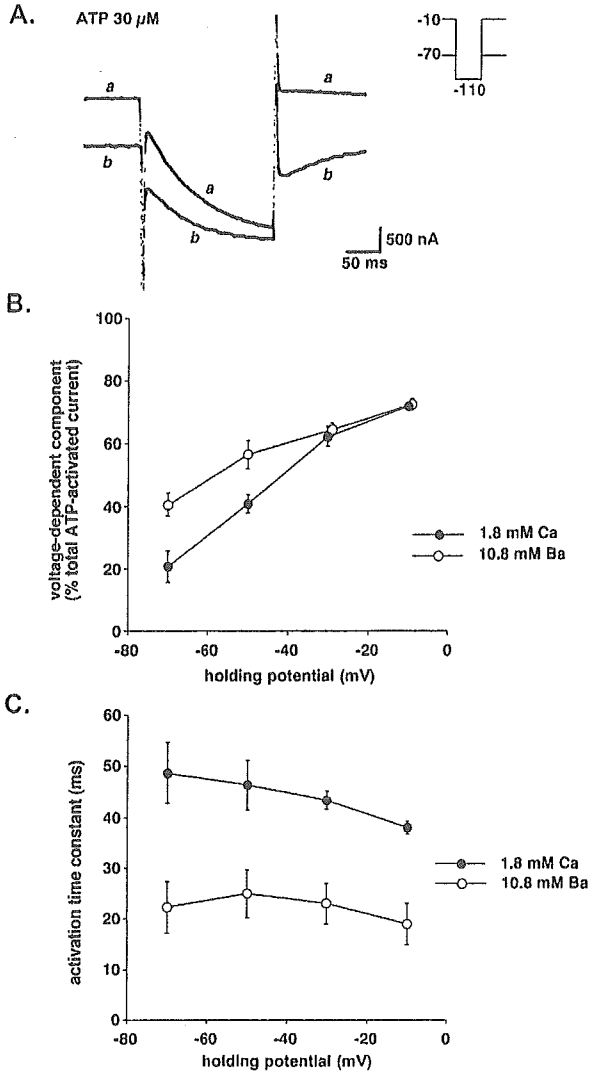

Fig. 2. Effect of holding potential on current. Current was evoked by 30 μM ATP. (A) Voltage-dependent current at −110 mV when stepped from a holding potential of −10 mV ("a") or −70 mV ("b"). (B) Effect of holding potential on voltage-dependent current. The amplitude of the voltage-dependent current was measured as described in Fig. 1A. Mean values obtained from 4 oocytes in a standard extracellular solution containing 1.8 mM Ca^{2+} (●) and an extracellular solution containing 10.8 mM Ba^{2+} (instead of Ca^{2+}; ○) were plotted. Bars represent the S.E.M. (C) Time course of activation of the voltage-dependent component. Time constants were determined as shown in Fig. 1B, and mean values obtained from 4 oocytes were plotted against holding potentials. Bars represent the S.E.M.

dependent component; the time constants were larger for 10 μM ATP than 30 μM ATP (Fig. 3C).

3.3. Activation and deactivation kinetics

Cl^- currents are observed in *Xenopus* oocytes (Weber, 1999; Zhang and Hamill, 2000). In the following experiments, current measurements were made using an extracellular solution containing 96 mM Na-aspartate instead of NaCl in order to facilitate the analysis of the voltage-dependent component of ATP-evoked current by reducing Cl^- currents. In doing so, there was an obvious reduction in outward current upon depolarization, resulting in better voltage-clamp conditions. Using this extracellular solution, the EC_{50} value for ATP-activated current measured at −50 mV was about 40 μM, which was lower than the value obtained with the standard extracellular solution containing 96 mM NaCl (about 100 μM; Nakazawa and Ohno, 2004). Fig. 4 illustrates

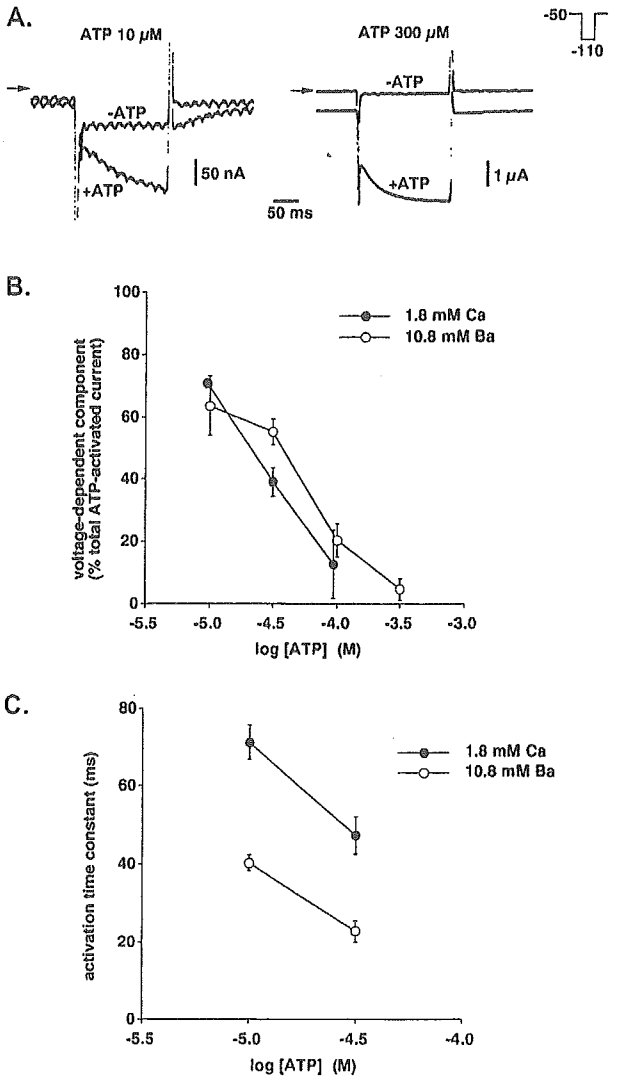

Fig. 3. Effect of ATP concentration. The voltage-dependent current was activated by hyperpolarization (−110 mV) from a holding potential of −50 mV. (A) Voltage-dependent current activated by 10 μM or 30 μM ATP. Current traces in the absence (−ATP) or presence (+ATP) of ATP are superimposed in each panel. (B) Contribution of the voltage-dependent current to total ATP-evoked current using different ATP concentrations. Mean values obtained from 4 oocytes in a standard extracellular solution containing 1.8 mM Ca^{2+} (●) and an extracelllular solution containing 10.8 mM Ba^{2+} (instead of Ca^{2+}; ○) were plotted. Bars represent the S.E.M. (C) Time course of activation of the voltage-dependent components. Time constants were determined as shown in Fig. 1B, and mean values obtained from 4 oocytes were plotted against holding potentials. Bars represent the S.E.M.

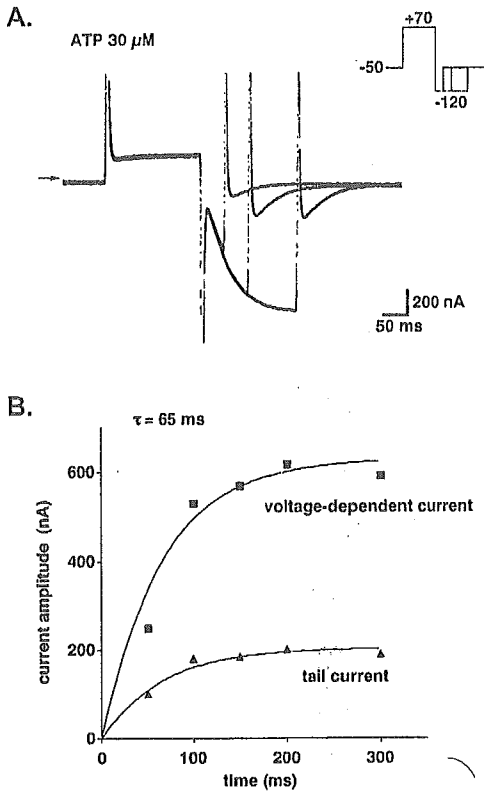

Fig. 4. Activation and tail current. (A) Gradual increase in magnitude of the tail current with increasing voltage-dependent current. Current traces obtained upon exposure to hyperpolarizing pulses (−120 mV) of different durations are superimposed. (B) Time course of activation of the voltage-dependent (■) and tail (▲) currents. Current amplitude was plotted against duration of hyperpolarization (also shown in panel A). The results of both time course activation experiments fit curves with a single time constant of 65 ms.

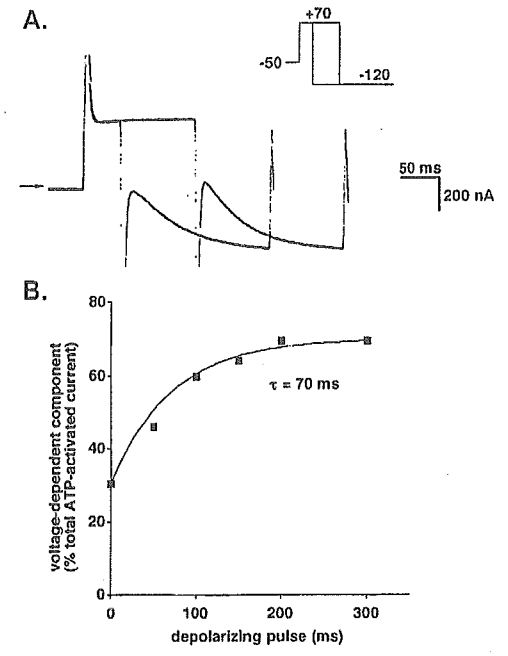

Fig. 5. Deactivation of the voltage-dependent component. (A) Current traces obtained using depolarizing pulses (+70 mV) of two different durations. The amplitude of the voltage-dependent component increased when the duration was prolonged. (B) Time course of deactivation of the voltage-dependent component. Current amplitude was plotted against duration of the depolarizing pulses (also shown in panel A).

the relation between activation kinetics of the voltage-dependent component and time course of tail current. As shown in Fig. 4A, oocytes were stepped to 70 mV and then to −120 mV to induce the voltage-dependent component. When hyperpolarization at −120 mV was terminated after various periods, a gradual increase in amplitude of the tail current was observed with increased duration of hyperpolarization at −120 mV. Time courses of both the voltage-dependent component and tail current could be fitted with curves with a single time constant (65 ms in this case; Fig. 4B). Similar fitting with single time constants were made for 4 oocytes tested, and the mean time constant±S.E.M. was 66.3±2.4 ms.

With increased duration of the +70 mV depolarizing pulse, increased amplitude of the voltage-dependent component was observed at −120 mV (Fig. 5A). This may reflect "deactivation" of the voltage-dependent component (Scheme 1):, where A is ATP, and R and R* are closed and open states, respectively, of the voltage-dependent component of $P2X_2$ receptor/channel. The deactivation time course could be fitted with a time constant of 70 ms in this case (Fig. 5B; mean±S.E.M., 71.3±1.3 ms; n=4).

3.4. Voltage dependence of activation and deactivation

As shown in Fig. 1, contribution of the voltage-dependent component to total ATP-evoked current was influenced by the holding potential prior to hyperpolarization. This was further examined by testing a number of prepulses at various potentials prior to hyperpolarization (Fig. 6A). As the prepulse became more depolarized, a greater contribution of the voltage-dependent component to total ATP-evoked current was observed, and this contribution became maximal near 0 mV (Fig. 6B). Thus, the voltage-dependent gate must be completely closed at potentials equal to or more positive than 0 mV. The data were fitted with a curve in accordance with the following model of "deactivation":

$$d_\infty = 1/\{1 + \exp[(E_{1/2} - E_m)/k]\}, \quad (1)$$

where d_∞ represents the relative proportion of closed gates at steady state, $E_{1/2}$ is the voltage at which the half-maximal closing occurs, E_m is the membrane potential, and

$$A{\cdot}R \underset{\text{(deactivation)}}{\overset{\text{(activation)}}{\rightleftharpoons}} A{\cdot}R^*$$

Scheme 1.

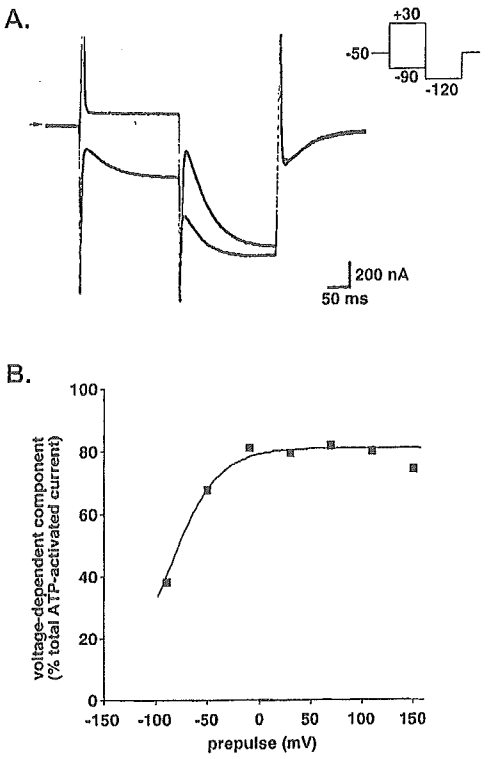

Fig. 6. Prepulse experiment. An ATP concentration of 30 μM was used. (A) Current traces obtained using prepulses of +30 mV ("a") or −90 mV ("b") prior to hyperpolarization at −120 mV. (B) Effect of prepulses. The relative contribution of the voltage-dependent current to total ATP-evoked current at −120 mV was plotted against each prepulse voltage. Some of this data is also shown in panel A.

k is a slope factor reflecting an energy barrier (Hodgkin and Huxley, 1952; Hille, 1992a). As shown in Fig. 6B, potential at which half the gates closed was estimated to be −90 mV in this case (mean±S.E.M., −78.8±5.2 mV; n=4).

The voltage dependence of activation was also examined. As shown in Fig. 7A, the channels responsible for the voltage-dependent component was sufficiently "deactivated" by applying a prepulse of +100 mV, and they were then activated at various hyperpolarization potentials. Contribution of the voltage-dependent component to total ATP-evoked current decreased as the hyperpolarization became more negative up to −45 mV in the case shown in Fig. 7B. Potentials exceeding −45 mV could not be examined since the resultant ATP-evoked current was not large enough to analyze. The data were fitted in accordance with the following model of "activation":

$$a_\infty = 1/\{1+\exp[(E_{1/2}-E_m)/k]\}, \quad (2)$$

where a_∞ represents the degree of gate opening at steady state. The other parameters are the same as those described above. The data obtained using Eq. (2) (Fig. 7B) could be fitted with a curve indicating that half of the gates were open at a potential of −30 mV.

The above data suggest that activation of the voltage-dependent gate occurs at more positive potentials than gate deactivation. To further investigate this, the fraction of the gates that escaped deactivation ($1-d_\infty$) was calculated from the data obtained during deactivation experiments. The deactivation data was then plotted alongside data obtained from activation experiments (Fig. 7C). These data suggest that the activation potential is 50 mV more positive than the deactivation potential.

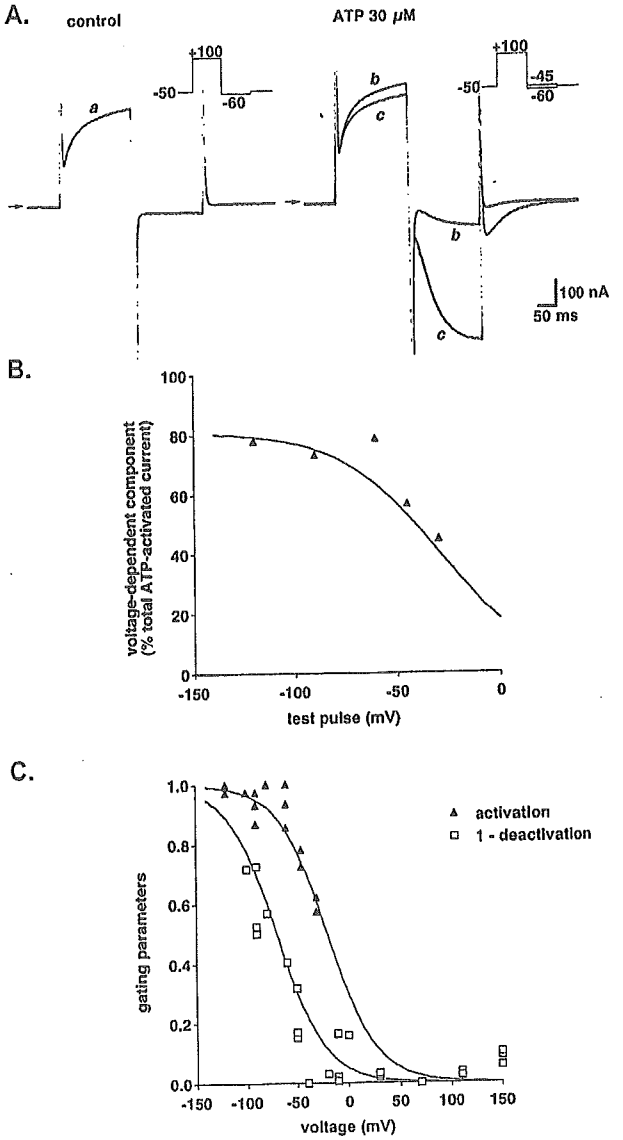

Fig. 7. Effect of hyperpolarization on voltage-dependent current. (A) Current traces before (control) and during the application of 30 μM ATP. In the panel on the right, two current traces obtained following hyperpolarization at −45 mV ("b") and −60 mV ("c") are superimposed. (B) Contribution of voltage-dependent current to total ATP-evoked current at various hyperpolarization potentials. Some of these data are shown in panel A. (C) Comparison of activation and deactivation. Parameters describing activation and deactivation were determined as described in the text. Each data point represents data obtained from individual oocytes.

4. Discussion

4.1. Schematic model of voltage-dependent gating

Recombinant $P2X_2$ receptor/channels expressed in *Xenopus* oocytes exhibited voltage-dependent gating properties similar to those of the channels in PC12 cells (Nakazawa et al., 1997b). The following similarities were observed: (1) the gate opens at negative potentials, (2) activation follows a time course with a time constant of 40 to 70 ms, and (3) gating depends on ATP concentrations. Thus, voltage-dependent gating in PC12 cells may be due to intrinsic expression of $P2X_2$ receptor/channels. We depict here a model that has been proposed to explain voltage-dependent gating of the channels in PC12 cells (Scheme 2):, where A is ATP, R_L and R_H represent closed states, and R* represents the open state (Nakazawa et al., 1997b). In this model, voltage-dependent gating is explained by transition between low and high ATP-affinity states. Upon hyperpolarization, there is a shift from the R_L to the R_H conformation. ATP preferentially binds to channels in the R_H state ($A \cdot R_H$), after which the channels open ($A \cdot R_H$*). Binding of ATP is the rate-limiting step since activation kinetics were observed to depend on ATP concentrations in the present study (Fig. 3C). The following rate constants have been proposed (Scheme 3): where k_{+1} parallels the concentration of ATP ($k_{+1}=k'_{+1}$[ATP]), and K_d is given by k_{-1}/k'_{+1} (Hille, 1992b). In the present experiment, an activation time constant of 65 ms was observed in the presence of 30 μM of ATP (Fig. 4), which is equivalent to a rate constant of 15 s^{-1}. Using these values, $k'_{+1}=k_{+1}/[ATP]=15\ s^{-1}/(30\ \mu M)=5\times10^5\ M^{-1}\ s^{-1}$. An inactivation time constant of 70 ms was observed in the presence of 30 μM of ATP (Fig. 5), which is equivalent to a rate constant of 14 s^{-1}. Thus, K_d was calculated to be $k_{-1}/k'_{-1}=14\ s^{-1}/(5\times10^5\ M^{-1}\ s^{-1})=28\ \mu M$, which is slightly less than the EC_{50} value obtained at −50 mV (about 40 μM). This estimation is in accordance with the finding that the voltage-dependent component is not completely activated at −50 mV (Fig. 7C). It is difficult to quantify the low-affinity ATP binding state since the relationship between concentration and response needs to be assessed at highly positive potentials, while $P2X_2$ receptor/channels permit only small current due to their inward-rectifying

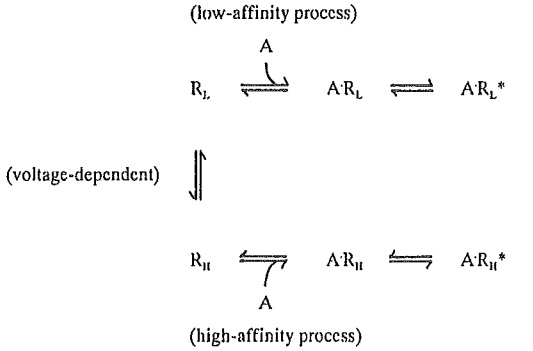

Scheme 2.

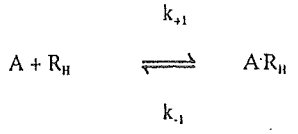

Scheme 3.

nature. We estimate here the low affinity from simple theoretical concentration–response curves. Fig. 8 shows two concentration–response curves. One demonstrates an EC_{50} of 30 μM, corresponding to a high-affinity state. If the other low-affinity state demonstrates an EC_{50} of 100 μM, more $P2X_2$ receptor/channels were in the high-affinity state in the presence of 10 μM ATP, and more were in the low-affinity state in the presence of 300 μM ATP. This is consistent with the greater observed contribution of the voltage-dependent component to total ATP-evoked current in the presence of 10 μM, while little was observed in the presence of 300 μM ATP (Fig. 3). Thus, the low-affinity state may be lower than the high-affinity state by threefold or larger.

The idea of the transition of $P2X_2$ receptor/channels between low- and high-affinity states might explain the "non-voltage-dependent" component of ATP-evoked current. For example, the current evoked by 30 μM ATP was not completely observed as voltage-dependent component even when activated at very negative potentials (Fig. 7B) or following deactivation at very positive potentials (Fig. 6B). This "non-voltage-dependent current" (about 20% of the total ATP-evoked current) might result from the activation of $P2X_2$ receptor/channels in the low-affinity state prior to voltage-dependent activation.

The voltage dependence of activation and deactivation differed, with deactivation occurring at more negative potentials (Fig. 7C). This indicates that the activation and the deactivation do not arise from a simple reversible "back-and-forth" process, rather, two voltage-dependent processes

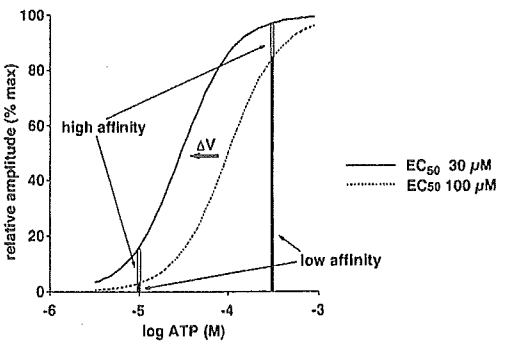

Fig. 8. Voltage-dependent change in sensitivity to ATP might explain dependence of the voltage-dependent current on ATP concentration. Low-affinity (EC_{50}=100 μM) and high-affinity (EC_{50}=30 μM) states of the receptor are thought to exist (Hill coefficient; 1.5). Each receptor shifts from a low-affinity to a high-affinity state upon hyperpolarization (ΔV). With 10 μM ATP, only a small proportion of the receptors, many of which were in the low-affinity state, were activated prior to hyperpolarization, but many more were activated upon induction of the high-affinity state by hyperpolarization. In the presence of 300 μM ATP, a larger proportion of the receptors were activated even in the low-affinity state, and induction of the high-affinity state caused only a marginal increase in activated receptors.

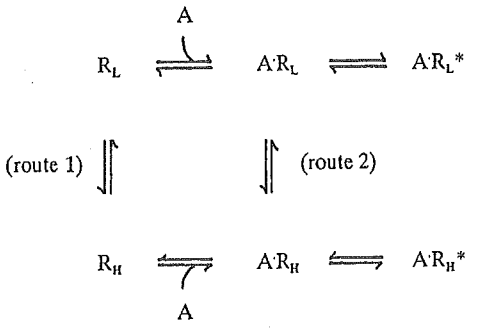

Scheme 4.

may be involved. We propose the following modification to Scheme 2.

This model (Scheme 4) involves two voltage-dependent processes, one resulting in activation through "route 1", and the other resulting in deactivation through "route 2". Such model would explain the observed difference in voltage dependence between activation and deactivation. However, we would expect this model to result in more difficult to interpret data than we did above based on Schemes 2 and 3.

4.2. Relevance of voltage-dependent gating

$P2X_2$ receptor is expressed in a number of neurons (e.g., Atkinson et al., 2000; Rubio and Soto, 2001). $P2X_2$ receptor/channel is permeable to Ca^{2+} (Egan and Khakh, 2004), and Ca^{2+} influx through the channel may influence cellular activity, although its exact role remains to be clarified. The voltage-dependent gating reported here may be relevant to the Ca^{2+} influx from the following consideration. Na^+ current (I_{Na}) and Ca^{2+} current (I_{Ca}) permeating through $P2X_2$ receptor/channel are:

$$I_{Na} = -P_{Na}\frac{E_m F^2}{RT}\frac{[Na]_o}{1-\exp(-EF/RT)} \quad (3)$$

$$I_{Ca} = -4P_{Ca}\frac{E_m F^2}{RT}\frac{[Ca]_o \exp(-2EF/RT)}{1-\exp(-2EF/RT)}, \quad (4)$$

where P_{Na} and P_{Ca} represent the permeability of Na^+ and Ca^{2+}, respectively, E_m represents the membrane potential, and F, R, and T are their usual physicochemical meanings (Fatt and Ginsborg, 1958; Nakazawa et al., 1989). The ratio of I_{Na} to I_{Ca} is thus:

$$\frac{I_{Ca}}{I_{Na}} = \frac{4P_{Ca}[Ca]_o}{P_{Na}[Na]_o}\frac{1}{\exp(E_m F/RT)[\exp(E_m F/RT)+1]} \quad (5)$$

This equation indicates that the ratio of I_{Ca}/I_{Na} is larger at more negative potentials. The ratio calculated at −90 mV is about 13-fold larger than that calculated at −30 mV. Thus, channel opening at negative potentials favors Ca^{2+} over Na^+ influx. Thus, voltage-dependent gating may facilitate cellular Ca^{2+}-dependent responses when cells are hyperpolarized. This may occur when efflux through K^+ channels outpaces depolarization afforded by opening of $P2X_2$ receptor/channels.

4.3. Conclusion

The results of the present study suggested that $P2X_2$ receptor exhibits voltage-dependent gating, and that this is not due to simple activation and deactivation of a single gate, but rather, due to a transition from a low ATP affinity to a high ATP affinity state. This may favor Ca^{2+} influx at negative potentials, although further studies are required to clarify the physiological significance of voltage-dependent gating of $P2X_2$ receptor.

Acknowledgements

This work was supported, in part, by a Health and Labour Science Research Grant for Research on Advanced Medical Technology from the Ministry of Health, Labour and Welfare, Japan, as well as a grant-in-aid for scientific research from the Ministry of Education, Science, Sports and Culture, Japan (KAKENHI 13672319) awarded to K.N.

References

Atkinson, L., Batten, T.F., Deuchars, J., 2000. $P2X_2$ receptor immunoreactivity in the dorsal vagal complex and area postrema of the rat. Neuroscience 99, 683–696.

Brake, A.J., Wagenbach, M.J., Julius, D., 1994. New structural motif for ligand-gated ion channels defined by an ionotropic ATP receptor. Nature 371, 519–523.

Clyne, J.D., LaPointe, L.D., Hume, R.I., 2002. The role of histidine residues in modulation of the rat $P2X_2$ purinoceptor by zinc and pH. J. Physiol. 539, 347–359.

Egan, T., Khakh, B.S., 2004. Contribution of calcium ions to P2X channel responses. J. Neurosci. 24, 3413–3420.

Egan, T.M., Haines, W.R., Voigt, M.M., 1998. A domain contributing to the ion channel of ATP-gated $P2X_2$ receptors identified by the substituted cysteine accessibility method. J. Neurosci. 18, 2350–2359.

Ennion, S., Hagan, S., Evans, R.J., 2000. The role of positively charged amino acids in ATP recognition by human $P2X_1$ receptors. J. Biol. Chem. 275, 29361–29367.

Fatt, P., Ginsborg, B.L., 1958. The ionic requirements for the production of action potentials in crustacean muscle fibres. J. Physiol. 142, 516–543.

Haines, W.R., Migita, K., Cox, J.A., Egan, T.M., Voigt, M.M., 2001. The first transmembrane domain of the P2X receptor subunit participates in the agonist-induced gating of the channel. J. Biol. Chem. 276, 32793–32798.

Hille, B., 1992a. Classical biophysics of the squid giant axon. Ionic channels of excitable membranes, Second Edition. Sinauer, Sunderland, MA, pp. 23–58.

Hille, B., 1992b. Ligand-gated channels of fast chemical synapses. Ionic channels of excitable membranes, Second Edition. Sinauer, Sunderland, MA, pp. 140–169.

Hodgkin, A.L., Huxley, A.F., 1952. The dual effect of membrane potential on sodium conductance in the giant axon of *Loligo*. J. Physiol. 116, 497–506.

Jiang, L.H., Rassendren, F., Surprenant, A., North, R.A., 2000. Identification of amino acid residues contributing to the ATP-binding site of a purinergic P2X receptor. J. Biol. Chem. 275, 34190–34196.

Jiang, L.H., Rassendren, F., Spelta, V., Surprenant, A., North, R.A., 2001. Amino acid residues involved in gating identified in the first membrane-spanning domain of the rat $P2X_2$ receptor. J. Biol. Chem. 276, 14902–14908.

Khakh, B.S., 2001. Molecular physiology of P2X receptors and ATP signalling at synapses. Nat. Rev. 2, 165–174.

Migita, K., Haines, W.R., Voigt, M.M., Egan, T.M., 2001. Polar residues of the second transmembrane domain influence cation permeability of the ATP-gated $P2X_2$ receptor. J. Biol. Chem. 276, 30934–30941.

Nakazawa, K., Ohno, Y., 1997. Effects of neuroamines and divalent cations on cloned and mutated ATP-gated channels. Eur. J. Pharmacol. 325, 101–108.

Nakazawa, K., Fujimori, K., Takanaka, A., Inoue, K., 1989. An ATP-activated conductance in pheochromocytoma cells and its suppression by extracellular calcium. J. Physiol. 428, 257–272.

Nakazawa, K., Liu, M., Inoue, K., Ohno, Y., 1997a. pH dependence of facilitation by neurotransmitters and divalent cations of $P2X_2$ purinoceptor/channels. Eur. J. Pharmacol. 337, 309–314.

Nakazawa, K., Liu, M., Inoue, K., Ohno, Y., 1997b. Voltage-dependent gating of ATP-activated channels in PC12 cells. J. Neurophysiol. 78, 884–890.

Nakazawa, K., Ojima, H., Ohno, Y., 2002. A highly conserved tryptophane residue indispensable for cloned rat neuronal P2X receptor activation. Neurosci. Lett. 324, 141–144.

North, R.A., 2002. Molecular physiology of P2X receptors. Physiol. Rev. 82, 1013–1067.

North, R.A., Surprenant, A., 2000. Pharmacology of cloned P2X receptors. Annu. Rev. Pharmacol. Toxicol. 40, 563–580.

Ralevic, V., Burnstock, G., 1998. Receptors for purines and pyrimidines. Pharmacol. Rev. 50, 413–492.

Rassendren, F., Buell, G., Newbolt, A., North, R.A., Surprenant, A., 1997. Identification of amino acid residues contributing to the pore of a P2X receptor. EMBO J. 16, 3446–3454.

Roberts, J.A., Evans, R.J., 2004. ATP binding at human $P2X_1$ receptors. Contribution of aromatic and basic amino acids revealed using mutagenesis and partial agonists. J. Biol. Chem. 279, 9043–9055.

Rubio, M., Soto, F., 2001. Distinct localization of P2X receptors at excitatory postsynaptic specializations. J. Neurosci. 21, 641–653.

Weber, W.-M., 1999. Ion currents of *Xenopus laevis* oocytes: state of the art. Biochim. Biophys. Acta 1421, 213–233.

Zhang, Y., Hamill, O.P., 2000. Calcium, voltage- and osmotic stress sensitive currents in *Xenopus* oocytes and their relationship to single mechanically gated channels. J. Physiol. 523, 83–99.

Novel mechanism of tumorigenesis: Increased transforming growth factor-β1 suppresses the expression of connexin 43 in BALB/cJ mice after implantation of poly-L-lactic acid

Saifuddin Ahmed, Toshie Tsuchiya
Division of Medical Devices, National Institute of Health Sciences, 1-18-1, Kamiyoga, Setagaya ku, Tokyo 158-8501, Japan

Received 15 December 2003; revised 24 March 2004; accepted 6 April 2004
Published online 4 June 2004 in Wiley InterScience (www.interscience.wiley.com). DOI: 10.1002/jbm.a.30090

Abstract: Poly-L-lactic acid (PLLA) is a widely used promising material for surgical implants such as tissue-engineered scaffolds. In this study, we aimed to determine the *in vivo* effect of PLLA plates on the cellular function of subcutaneous tissue in the two mouse strains, BALB/cJ and SJL/J, higher and lower tumorigenic strains, respectively. Gap-junctional intercellular communication (GJIC) and the expression of connexin 43 (Cx43) protein were significantly suppressed, whereas the secretion of transforming growth factor-β1 (TGF-β1) level was significantly increased in PLLA-implanted BALB/cJ mice compared with BALB/cJ controls. However, no significant difference in TGF-β1 secretion was observed between the SJL/J-implanted and SJL/J control mice. We found for the first time that a significant difference was observed between the two strains; thus, the PLLA increased the secretion of TGF-β1 and suppressed the mRNA expression of Cx43 at the earlier stage after implantation into the higher-tumorigenic strain, BALB/cJ mice. This novel mechanism might have a vital role in the inhibition of GJIC and promote the tumorigenesis in BALB/cJ mice. © 2004 Wiley Periodicals, Inc. J Biomed Mater Res 70A: 335–340, 2004

Key words: poly-L-lactic acid; gap-junctional intercellular communication (GJIC); connexin 43; transforming growth factor (TGF)-β; tumorigenesis

INTRODUCTION

The implantation of a biomaterial always induces a host inflammatory response. The extent and resolution of these responses have a vital role in determining the long-term success of implanted medical devices.[1–3] Poly-L-lactic acid (PLLA) is a widely used material for surgical implants and clinically as a bioabsorbable suture material.[4,5] Polyurethanes (PUs) have also been used for implant applications because of their useful elastomeric properties and high tensile strength, lubricity, and good abrasion resistance. Some adverse effects of the biomaterials, such as PLLA and PUs, have been reported in animal experiments. Long-term implants of PLLA produced tumorigenicity in rats.[6] Different kinds of PUs induced various tumor incidences in rats.[7] All tumors have been generally viewed as the outcome of disruption of the homeostatic regulation of the cellular ability to respond to extracellular signals, which trigger intracellular signal transduction abnormalities.[8] During the evolutionary transition from the single-cell organism to the multicellular organism, many genes appeared to accompany these cellular functions. One of these genes was the gene coding for a membrane-associated protein channel (the gap junction).[9] Gap-junctional intercellular communications (GJIC) are transmembrane channels that allow the cell–cell transfer of small molecules and are composed of protein subunits known as connexin; at least 19 connexins exist and they are expressed in a cell- and development-specific manner.[10,11] GJIC also has an important role in the maintenance of cell homeostasis and in the control of cell growth.[12] So, the loss of GJIC has been considered to cause abnormal development and tumor formation.[13–15] Several tumor promoters have been shown to restrict GJIC by phosphorylation of connexin proteins, such as connexin 43 (Cx43), which is an essential

Correspondence to: T. Tsuchiya; e-mail: tsuchiya@nihs.go.jp
Contract grant sponsor: Health and Labour Sciences Research Grants
Contract grant sponsor: Research on Advanced Medical Technology, Ministry of Health, Labour and Welfare
Contract grant sponsor: Japan Health Sciences Foundation

protein to form the gap-junction channel.[16,17] We have hypothesized that the different tumorigenic potentials of PLLA and PUs are caused mainly by the different tumor-promoting activities of these biomaterials. Therefore, we investigated the effects of PLLA on the subcutaneous tissue between the two strains of female mice, BALB/cJ and SJL/J.

MATERIALS AND METHODS

Animals

Five-week-old female BALB/cJ and SJL/J mice were purchased from Charles River (Japan) and maintained in the animal center according to the animal welfare National Institute of Health Sciences guidance. All mice were fed with standard pellet diets and water *ad libitum*, before and after the implantation.

Implantation of PLLA

PLLA was obtained from Shimadzu Co. Ltd. as uniform plates. Implants (size: 20 × 10 × 1 mm, weight-average molecular weight 200,000) were sterilized using ethylene oxide gas before use. Sodium pentobarbital (4 mg/kg) was intraperitoneally administered to the mice. The dorsal skin was shaved and scrubbed with 70% alcohol. Using an aseptic technique, an incision of approximately 2 cm was made; away from the incision, a subcutaneous pocket was formed by blunt dissection, and one piece of PLLA was placed in the pocket. The incision was closed with silk threads. In both strains, controls were obtained by sham operation and subsequent subcutaneous pocket formation. After surgery, the mice were housed in individual cages. After 30 days, mice from the implanted group were sacrificed, implanted materials were excised out, and subcutaneous tissues from the adjacent sites were collected for culture. At the same time, subcutaneous tissues were removed from the sites in the sham-operated controls that correlated with the implant sites.

Cell culture of subcutaneous tissues

The subcutaneous tissues were maintained in minimum essential medium supplemented with 10% fetal bovine serum in a 5% CO_2 atmosphere at 37°C.

Scrape-loading and dye transfer (SLDT) assay

SLDT technique was performed by the method of El-Fouly et al.[18] Confluent monolayer cells in 35-mm culture dishes were used. After rinsing with Ca^{2+} Mg^{2+} phosphate-buffered saline [PBS (+)], cell dishes were loaded with 0.1% Lucifer Yellow (Molecular Probes, Eugene, OR) in PBS (+) solution and were scraped immediately with a sharp blade. After incubation for 5 min at 37°C, cells were washed three times with PBS (+) and the extent of dye transfer was monitored using a fluorescence microscope, equipped with a type UFX-DXII CCD camera and super high-pressure mercury lamp power supply (Nikon, Tokyo, Japan).

Western blot analysis

When cells grew confluently in 60-mm tissue culture dishes, all cells were lysed directly in 100 μL of 2% sodium dodecyl sulfate (SDS) gel loading buffer (50 m*M* Tris-HCl, pH 6.8, 100 m*M* 2-mercaptoethanol, 2% SDS, 0.1% bromophenol blue, 10% glycerol). The protein concentration of the cleared lysate was measured using the microplate BCA (bicinchoninic acid) protein assay (Pierce, Rockford, IL). Equivalent protein samples were analyzed by 7.5% SDS–polyacrylamide gel electrophoresis. The proteins were transferred to Hybond-ECL nitrocellulose membranes (Amersham Pharmacia Biotech UK Ltd., Buckinghamshire, UK). Cx43 protein was detected by anti-Cx43 polyclonal antibodies (ZYMED Laboratories, Inc., San Francisco, CA). The membrane was soaked with Block Ace (Yukijirusi Nyugyo, Sappro, Japan), reacted with the anti-Cx43 polyclonal antibodies for 1 h, and after washes with PBS containing 0.1% Tween20, reacted with the secondary anti-rabbit immunoglobulin G antibody conjugated with horseradish peroxidase for 1 h. After several washes with PBS–Tween20, the membrane was detected with the ECL detection system (Amersham Pharmacia Biotech UK Ltd.).

Reverse transcriptase polymerase chain reaction (RT-PCR)

Cx43 mRNA expression was verified by RT-PCR. Total cellular RNA was isolated from cultured cells in Trizol reagent (Life Technologies, Inc., Frederick, MD) following the manufacturer's instructions. The concentration of total RNA was determined using a UV spectrophotometer (Gene Quant; Pharmacia Biotech, Piscataway, NJ). cDNA was synthesized from 1 μg of total RNA by RT using the First-Strand cDNA synthesis kit (Amersham Pharmacia Biotech, Uppsala, Sweden). Amplification was performed in a volume of 25 μL containing 1 μL of cDNA, 10 pmol of each primer, 0.625 unit of *Taq* polymerase (Promega, Madison, WI) and 0.2 m*M* of each deoxynucleotide triphosphate. The sequence of the primer pairs were as follows: forward 5′-ACAGTCTGCCTTTCGCTGTAAC-3′ and reverse 5′-GTAAGGATCGCTTCTTCCCTTC-3′. The PCR cycle was as follows: initial denaturation at 94°C for 5 min, followed by 25 cycles of 94°C for 1 min, 60°C for 1 min, and 72°C for 1 min, with final extension at 72°C for 7 min. The amplified product was separated on 1.5% agarose gel and visualized with SYBR Green I (BioWhittaker Molecular Applications, Rockland, ME). For relative quantitation, the signal intensity of each lane was standardized to that of a housekeeping gene,

GAPDH. To amplify this gene, the following primer pairs were used: forward 5′-CCCATCACCATCTTCCAGGAGC-GAGA-3′ and reverse 5′-TGGCCAAGGTCATCCATGA-CAACTTTGG-3′.

Enzyme-linked immunosorbent assay (ELISA)

Cells were seeded onto 60-mm dishes. The conditioned medium was collected and obtained after the centrifugation at 1000 rpm for 2 min. The transforming growth factor (TGF)-β levels of the media were measured with commercially available ELISA kits (R&D Systems Inc., Minneapolis, MN).

Cytokine treatment

Here, we used sham-operated BALB/cJ mice cells as a control. One hundred thousand cells were seeded onto 35-mm tissue culture dishes and cultured. After 4 h seeding in a 5% CO_2 atmosphere at 37°C, cells were treated with TGF-β1 (0, 2, and 10 ng/mL). Thereafter, SLDT and RT-PCR were performed. Purified human TGF-β1 was purchased from R&D Systems.

Statistical analysis

Student *t* test was used to compare the implanted samples with the controls. Statistical significance was accepted at $p < 0.05$. Values were presented as the mean ± standard deviation.

RESULTS AND DISCUSSION

There are many known tumorigenesis-inducing factors. It was reported that many plastics induce malignant tumors when implanted subcutaneously into rats and mice.[19–22] PLLA shows slow degradation, and therefore has been applied as a biomaterial for surgical devices such as bone plates, pins, and screws. It was reported in different studies that polyetherurethane, polyethylene, and PLLA produced tumors in rats.[6,7,23–25] In our study, tumors were induced by PLLA plates in BALB/cJ mice at 100% incidence but not in SJL/J mice at the surrounding tissues of PLLA plates during a 10-month *in vivo* study. To understand the mechanisms of tumorigenesis induced by PLLA, we focused on the inhibitory effects on GJIC at the early stage of tumorigenesis. To assess functional GJIC, the SLDT assay was performed. Brand et al.[26] reported that BALB/cJ mice are a higher and SJL/J mice are a lower tumorigenic strain. Our present results showed that the GJIC was significantly inhibited in 1-month PLLA-implanted BALB/cJ mice cells compared with BALB/cJ controls (Fig. 1). In contrast, no significant difference was observed between the 1-month PLLA-implanted SJL/J mice and SJL/J controls (Fig. 1). The data also revealed that the dye migration was higher in control BALB/cJ mice than control SJL/J mice (Fig. 1). High responder to the tumorigenicity may be classified as animals that are easily suppressed in both GJIC function and the connexins expression. This perturbed gap junction is likely to have a major role in the PLLA-induced tumorigenesis. Gap junctions are also regulated by the posttranslational phosphorylation of the carboxy-terminal tail region on the connexin molecule. Phosphorylation of connexin molecules is closely related with the inhibition of GJIC.[27,28] Phosphorylation has been involved in controlling a broad variety of connexin processes that include trafficking, gathering/nongathering, degradation, and also the gating of gap channels. It was also reported that communication-deficient cells did not express the Cx43–biphosphorylated (P_2) isoform but cells with low gap-junction permeability showed detectable amounts of the Cx43–monophosphorylated (P_1) isoform.[16] To survey the cause, we examined the mRNA and protein expression of the Cx43 gene. Here, mRNA expression was suppressed in PLLA-implanted BALB/cJ mice compared with BALB/cJ controls [Fig. 2(A)]. No significant difference was observed between the PLLA-implanted SJL/J mice and SJL/J controls [Fig. 2(B)]. We also found that the total level of protein expression such as unphos-

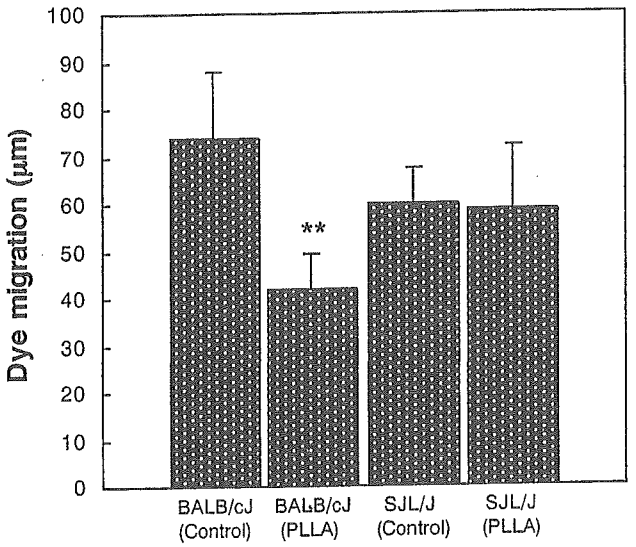

Figure 1. Statistical analysis of the SLDT assay. In both the implanted and sham-operated controls, three mice of each strain were sacrificed after 30 days. Results shown are representative of two independent experiments. GJIC was significantly inhibited in PLLA-implanted BALB/cJ mice cells compared with BALB/cJ controls. $^{**}p < 0.01$.

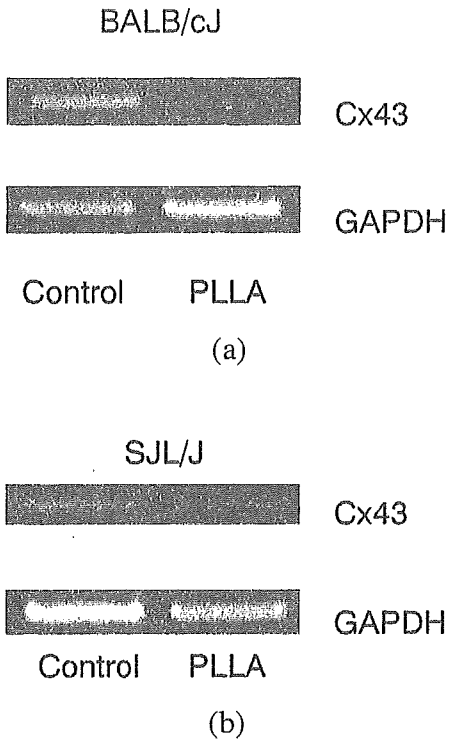

Figure 2. mRNA expression of Cx43 by RT-PCR analysis. In both the implanted and sham-operated controls, three mice of each strain were sacrificed after 30 days. Results shown are representative of two independent experiments. SYBR Green I stained PCR products after agarose gel electrophoresis showed that (A) mRNA expression was suppressed in PLLA-implanted BALB/cJ mice compared with BALB/cJ controls, and (B) no significant difference was observed between the PLLA-implanted SJL/J mice and SJL/J controls.

phorylated (P_0), P_1, and P_2 levels were significantly decreased in PLLA-implanted BALB/cJ mice compared with the control (Fig. 3). Asamoto et al.[29] reported that tumorigenicity was enhanced when the expression of Cx43 protein was suppressed by the anti-sense RNA of Cx43. A similar tendency was also observed in our study where the protein expression might be inhibited via down-regulation of the mRNA level. The genetic alteration and posttranslational

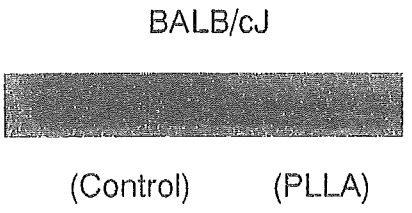

Figure 3. Protein expression of Cx43 by Western blot analysis. In both the implanted and sham-operated controls, three mice of each strain were sacrificed after 30 days. Results shown are representative of two independent experiments. Total level of protein expression such P_0, P_1, and P_2 levels were significantly decreased in PLLA-implanted BALB/cJ mice compared with the controls.

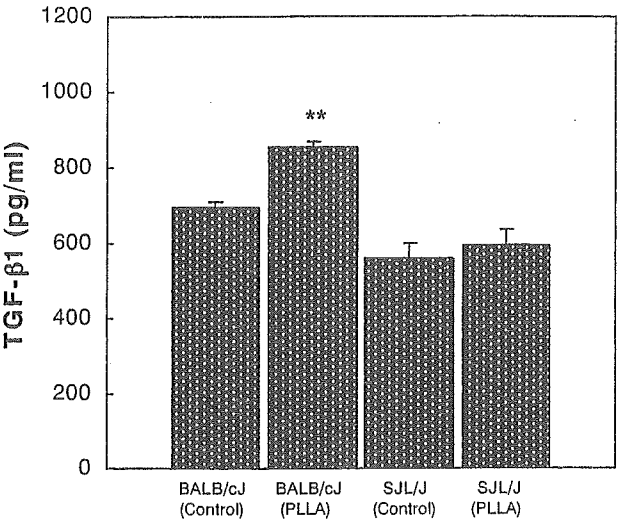

Figure 4. Statistical analysis of TGF-β1 cytokine assay by ELISA. In both the implanted and sham-operated controls, three mice of each strain were sacrificed after 30 days. Results shown are representative of two independent experiments. Secretion of the TGF-β1 level was significantly increased in PLLA-implanted BALB/cJ mice compared with BALB/cJ controls. $^{**}p < 0.01$.

modification in the Cx43 protein was shown to be involved in impaired GJIC and could be associated with tumorigenesis. Therefore, it is suggested that the inhibitory effect of PLLA on GJIC might be caused by the alteration in the Cx43 protein, causing enhancement of tumorigenesis. Moreover, Moorby and Patel[30] reported a direct action of the Cx43 protein on cell growth that was mediated via the cytoplasmic carboxyl domain.

Because TGF-β1 inhibits GJIC by decreasing the phosphorylated form of Cx43[31] and the phosphorylation of Cx43 has been implicated in gap-junction assembly and gating events,[16,27,32] we hypothesized that TGF-β1 might have an important role on PLLA-implanted BALB/cJ mice. Figure 4 clearly demonstrates that the secretion of the TGF-β1 level was significantly increased in PLLA-implanted BALB/cJ subcutaneous tissue in comparison with those from BALB/cJ control mice. No significant difference was found in the secretion of TGF-β1 between the SJL/J implanted and SJL/J control mice. TGF-β2 and TGF-β3 cytokine assay revealed no significant difference in TGF-β2 secretion and TGF-β3 was below the detection level (data not shown). So we performed an *in vitro* study, which showed that the intercellular communication and the mRNA expression of Cx43 were significantly suppressed in BALB/cJ control cells when treated with TGF-β1 [Fig. 5(A,B)].

In conclusion, we suggest that increased secretion of TGF-β1 (Fig. 4) suppressed expression of the gap-junctional protein Cx43 (Fig. 3) at the earlier stage after implantation of PLLA in BALB/cJ mice, resulting in

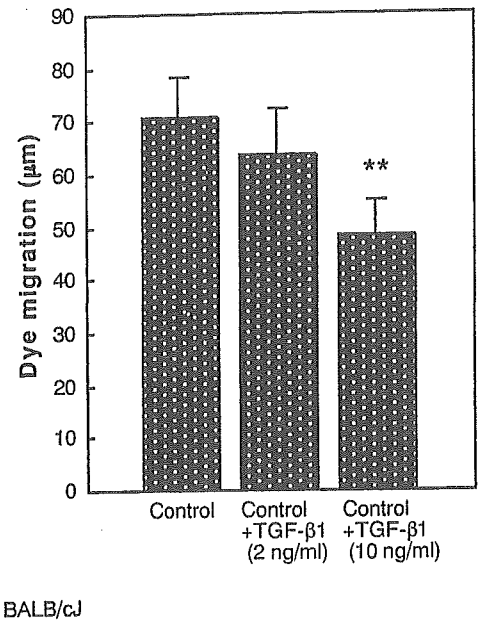

(a)

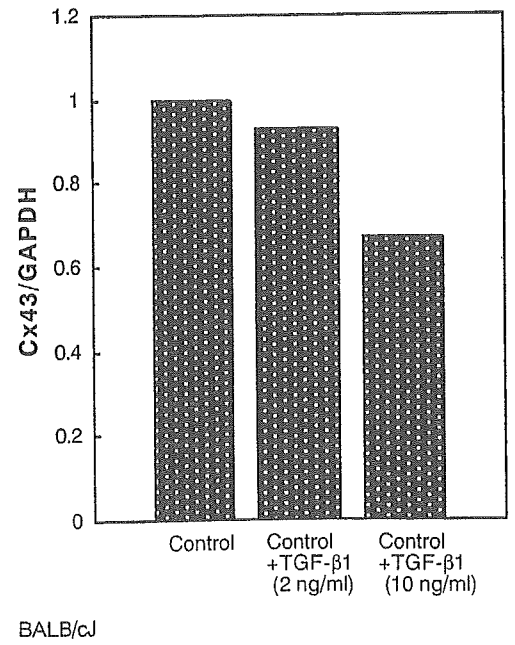

(b)

Figure 5. (A) SLDT assay. (B) National Institutes of Health image analysis quantitation of RT-PCR bands. In both figures, BALB/cJ control cells were treated with 2 and 10 ng/mL TGF-β1. GJIC was significantly inhibited and mRNA expression was significantly suppressed in BALB/cJ control cells treated with 10 ng/mL TGF-β1 compared with BALB/cJ controls. $^{**}p < 0.01$. Three dishes were used for one data point (bar) as one experiment. Results shown are representative of two independent experiments.

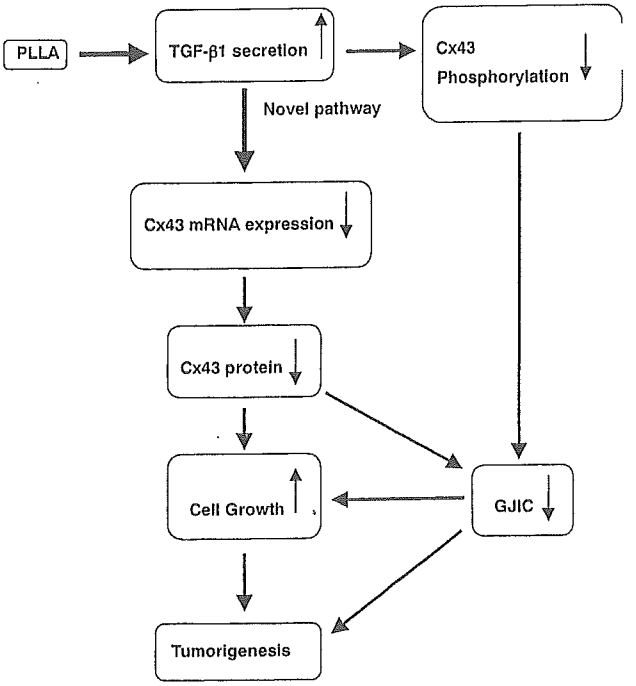

Figure 6. Schematic representation of the pathway of tumorigenesis induced by PLLA in BALB/cJ mice.

the suppression of the function of GJIC (Fig. 1) and at the same time, mRNA expression of Cx43 was suppressed in BALB/cJ mice (higher tumorigenic) but not in SJL/J mice (lower tumorigenic) [Fig. 2(A,B)]. TGF-β1 also suppressed the expression of mRNA of Cx43 and the function of GJIC in the BALB/cJ mouse cells *in vitro* [Fig. 5(A,B)]. These results indicated the novel mechanism of tumorigenesis induced by PLLA (Fig. 6).

References

1. Tang L, Eaton JW. Inflammatory responses to biomaterials. Am J Clin Pathol 1995;103:466–471.
2. Rames A, Williams DF. Immune response in biocompatibility. Biomaterials 1992;13:731–743.
3. Anderson JM. Mechanisms of inflammation and infection with implanted devices. Cardiovasc Pathol 1993;2:33s–41s.
4. Kulkarni RK, Pani KC, Neuman C, Leonard F. Polylactic acid for surgical implants. Arch Surg 1966;93:839–843.
5. Craig PH, Williams JA, Davis KW, Magoun AD, Levy AJ, Bogdansky S, Jones JP Jr. A biological comparison of polyglactin 910 and polyglycolic acid synthetic absorbable sutures. Surg Gynecol Obstet 1995;141:1–10.
6. Nakamura T, Shimizu Y, Okumura N, Matsui T, Hyon SH, Shimamoto T. Tumorigenicity of poly-L-lactide (PLLA) plates compared with medical-grade polyethylene. J Biomed Mater Res 1994;28:17–25.
7. Nakamura A, Kawasaki Y, Takada K, Aida Y, Kurokama Y, Kojima S, Shintani H, Matsui M, Nohmi T, Matsuoka A, Sofuni T, Kurihara M, Miyata N, Uchima T, Fujimaki M. Difference in tumor incidence and other tissue responses to polyetherurethanes and polydimethylsiloxane in long-term subcutaneous implantation into rats. J Biomed Mater Res 1992;26:631–650.

8. Trosko JE, Madhukar BV, Chang CC. Endogenous and exogenous modulation of gap junctional intercellular communication: toxicological and pharmacological implications. Life Sci 1993;53:1–19.
9. Trosko JE, Ruch RJ. Cell–cell communication in carcinogenesis. Front Biosci 1998;3:D208–236.
10. Eiberger J, Degen J, Romualdi A, Deutsch U, Willecke K, Sohl G. Connexin genes in the mouse and human genome. Cell Commun Adhes 2001;8:163–165.
11. Bruzzone R, White TW, Paul DL. Connections with connexins: the molecular basis of direct intercellular signaling. Eur J Biochem 1996;238:1–27.
12. Loewenstein WR. Junctional intercellular communication and the control of growth. Biochim Biophys Acta 1979;560:1–65.
13. Guthrie SC, Gilula NB. Gap junctional communication and development. Trends Neurosci 1989;12:12–16.
14. Klaunig JE, Ruch RJ. Role of inhibition of intercellular communication in carcinogenesis. Lab Invest 1990;62:135–146.
15. Mesnil M, Yamasaki H. Cell–cell communication and growth control of normal and cancer cells: evidence and hypothesis. Mol Carcinog 1993;7:14–17.
16. Musil LS, Goodenough DA. Biochemical analysis of connexin43 intracellular transport, phosphorylation, and assembly into gap junctional plaques. J Cell Biol 1991;115:1357–1374.
17. Musil LS, Goodenough DA. Multisubunit assembly of an integral plasma membrane channel protein, gap junction connexin43, occurs after exit from the ER. Cell 1993;74:1065–1077.
18. El-Fouly MH, Trosko JE, Chang CC. Scrape-loading and dye transfer. A rapid and simple technique to study gap junctional intercellular communication. Exp Cell Res 1987;168:422–430.
19. Turner FC. Sarcomas at sites of subcutaneously implanted bakelite disks in rats. J Natl Cancer Inst 1941;2:81–83.
20. Oppenheimer BS, Oppenheimer ET, Danishefsky I, Stout AP, Eirich FR. Further studies of polymers as carcinogenic agents in animals. Cancer Res 1955;15:333–340.
21. Bischoff F, Bryson G. Carcinogenesis through solid state surface. Prog Exp Tumor Res 1964;5:85–133.
22. Karp RD. Tumorigenesis by Millipore filters in mice: histology and ultrastructure of tissue reactions as related to pore size. J Natl Cancer Inst 1973;51:1275–1285.
23. Tsuchiya T, Hata H, Nakamura A. Studies on the tumor-promoting activity of biomaterials: inhibition of metabolic cooperation by polyetherurethane and silicone. J Biomed Mater Res 1995;29:113–119.
24. Tsuchiya T. A useful marker for evaluating tissue-engineered products: gap-junctional communication for assessment of the tumor-promoting action and disruption of cell differentiation in tissue-engineered products. J Biomater Sci Polym Ed 2000; 11:947–959.
25. Nakaoka R, Tsuchiya T, Kato K, Ikada Y, Nakamura A. Studies on tumor-promoting activity of polyethylene: inhibitory activity of metabolic cooperation on polyethylene surfaces is markedly decreased by surface modification with collagen but not with RGDS peptide. J Biomed Mater Res 1997;35:391–397.
26. Brand I, Buoen LC, Brand KG. Foreign-body tumors of mice: strain and sex differences in latency and incidence. J Natl Cancer Inst 1977;58:1443–1447.
27. Musil LS, Cunningham BA, Edelman GM, Goodenough DA. Differential phosphorylation of the gap junction protein connexin43 in junctional communication-competent and -deficient cell lines. J Cell Biol 1990;111:2077–2088.
28. Lampe PD, Lau AF. Regulation of gap junctions by phosphorylation of connexins. Arch Biochem Biophys 2000;384:205–215.
29. Asamoto M, Toriyama-Baba T, Krutovskikh V, Cohen SM, Tsuda H. Enhanced tumorigenicity of rat bladder squamous cell carcinoma cells after abrogation of gap junctional intercellular communication. Jpn J Cancer Res 1998;89:481–486.
30. Moorby C, Patel M. Dual functions for connexins: Cx43 regulates growth independently of gap junction formation. Exp Cell Res 2001;271:238–248.
31. Wyatt LE, Chung CY, Carlsen B, Iida-Klein A, Rudkin GH, Ishida K, Yamaguchi DT, Miller TA. Bone morphogenetic protein-2 (BMP-2) and transforming growth factor-beta1 (TGF-beta1) alter connexin 43 phosphorylation in MC3T3-E1 cells. BMC Cell Biol 2001;2:14.
32. Laird DW, Castillo M, Kasprzak L. Gap junction turnover, intracellular trafficking, and phosphorylation of connexin43 in brefeldin A-treated rat mammary tumor cells. J Cell Biol 1995; 131:1193–1203.

Original Paper

International Archives of Allergy and Immunology

Int Arch Allergy Immunol 2004;135:3–11
DOI: 10.1159/000080036

Received: December 23, 2003
Accepted after revision: June 7, 2004
Published online: July 29, 2004

Proteomic Analysis of Putative Latex Allergens

Takeshi Yagami[a] Yuji Haishima[a] Toshie Tsuchiya[a]
Akiko Tomitaka-Yagami[b] Hisao Kano[b] Kayoko Matsunaga[b]

[a]Division of Medical Devices, National Institute of Health Sciences, Tokyo, [b]Department of Dermatology, Fujita Health University School of Medicine, Toyoake, Japan

Key Words
Proteomics · Allergenomics · Latex allergy · Allergen · Two-dimensional gel electrophoresis · Immunoblotting · In-gel digestion · Mass spectrometry · Database search

Abstract
Background: Extensive analysis of allergenic proteins is generally time-consuming and labor-intensive. Accordingly, a rapid and easy procedure for allergen identification is required. As sequence information on proteins and genes is accumulated in databases, it is becoming easier to identify a candidate protein using proteomic strategies, i.e. two-dimensional gel electrophoresis, site-specific fragmentation, mass spectrometry and then database search. In this study, we evaluated the usefulness of a proteomic strategy for identifying putative allergens through its application to latex proteins. ***Methods:*** Latex proteins were separated with two-dimensional gel electrophoresis, and putative allergens were visualized by IgE immunoblotting using pooled serum from latex-sensitive patients. The IgE-interactive proteins were cut out from the negatively stained two-dimensional gel and subjected to in-gel digestion by trypsin. Then the resulting peptides were analyzed with mass spectrometry. Based on the mass spectrometric data we obtained, the allergen candidates were assigned by a database search. ***Results:*** Five previously reported allergens and five new allergen candidates were identified with the proteomic approach without isolating the individual proteins. Less than 1 mg of crude latex protein was sufficient for the entire protocol. Because plural proteins can be processed in parallel, analysis of about 50 IgE-interactive proteins was accomplished within 1 week. ***Conclusions:*** Analysis of putative allergens with proteomic strategies (allergenomics) is a promising avenue for rapid and exhaustive research. The high resolving power of two-dimensional gel electrophoresis is superior to conventional gel electrophoresis. Moreover, the notable sensitivity and speed of mass spectrometry have pronounced advantages over the N-terminal sequencing that has generally been used for protein identification.

Introduction

Latex allergy has become a serious problem in medical settings since the late 1980s [1]. Intensive research on allergenic proteins responsible for this immediate-type hypersensitivity has revealed 13 officially registered latex allergens to date. It is notable that many of the latex allergens have something to do with the defense mechanisms of the rubber tree [2–6]. Defense-related proteins of higher plants are relatively conserved in the course of evolu-

KARGER
Fax + 41 61 306 12 34
E-Mail karger@karger.ch
www.karger.com

1018–2438/04/1351–0003$21.00/0

Accessible online at:
www.karger.com/iaa

Correspondence to: Dr. Takeshi Yagami
Division of Medical Devices, National Institute of Health Sciences
Kamiyoga 1-18-1, Setagaya-ku
Tokyo 158-8501 (Japan)
Tel. +81 3 3700 4842, Fax +81 3 3707 6950, E-Mail yagami@nihs.go.jp

tion and therefore share the partial sequences indispensable for their function. Such a conserved sequence is sometimes called a functional domain. For example, hevein is one of the major latex allergens and contains a chitin-binding domain that is indispensable for its antifungal activity. A homologous chitin-binding domain has already been found in several antifungal proteins from various plant species. Class I chitinase is a representative containing a hevein-like domain. Because of this shared domain, class I chitinase is expected to be allergenic for hevein-sensitized patients [4–6]. Cross-reactivity between class I chitinase and hevein was indeed confirmed by several research groups [7, 8]. However, hevein cannot explain all of the cross-reactions of latex-allergic people to a wide range of fruits and vegetables (latex-fruit syndrome). Other undiscovered minor cross-reactive latex allergens must play a role in the latex-fruit syndrome. We need a powerful methodology in order to investigate such minor but significant allergens as well as major but hidden allergenic proteins.

As sequence data of proteins and genes are accumulated in databases, it is becoming easy to analyze candidate proteins rapidly and comprehensively using an effective separation technique coupled with mass spectrometry [9, 10]. This new strategy, aiming at comprehensive analysis of total proteins (proteome) in a cell or tissue, is now referred to as 'proteomics'. For the application of proteomic strategies to allergenic proteins in particular, the term 'allergenomics' has been proposed. In conventional approaches, we needed to isolate each allergenic protein to identify and fully characterize it. This process is usually complex, time-consuming and labor-intensive. However, in allergenomics, complex protein mixtures are effectively resolved with two-dimensional gel electrophoresis or the equivalent, and IgE-interactive proteins are detected by subsequent immunoblotting using pooled patients' serum. We can easily identify putative allergens through their site-specific degradation and the subsequent mass spectrometric analysis of the fragmented peptides and database search. The overall procedure is expected to be quicker and less labor-intensive than any procedures used to date. Moreover, we can analyze numerous IgE-interactive proteins in parallel. Semiautomatic analysis of allergen candidates is also possible. From these features, allergenomics is expected to be a key technique for fast, effective and comprehensive analysis of IgE-interactive proteins.

A few examples of the application of proteomic strategies to pollen allergens have been published in recent years [11, 12]. However, the effectiveness of allergenomics has not been fully demonstrated yet. In this study, we evaluated the usefulness of allergenomics through the analysis of latex proteins. Latex allergens have been extensively studied using traditional biochemical methods [1]. Nevertheless, minor latex allergens that have been overlooked and new cross-reactive allergens pertinent to the latex-fruit syndrome remain to be scrutinized. The advantages of allergenomics in analyzing these troublesome allergens are demonstrated below.

Subjects and Methods

Subjects

Six latex-sensitive patients and four control volunteers provided their serum for this study. Latex-allergic patients (table 1) were diagnosed from their clinical history of allergy to natural rubber-containing products, positive results of a skin prick test (SPT) using crude extract of latex proteins [13] and scores from a latex-specific IgE radioallergosorbent test (CAP RAST, Pharmacia Diagnostics). When a subject with a convincing clinical history of latex allergy did not show positive reactions on the SPT, a gradual provocation test to a brand of highly allergenic latex gloves was carried out for definite diagnosis. Three of the control subjects were medical personnel who are exposed constantly to various kinds of products made from natural rubber. One control subject was a homemaker suffering from erythema nodosum but with no background of allergies. They were confirmed not to have a latex allergy from the diagnostic criteria mentioned above. Informed consent was obtained from all of the participants before collecting their blood.

Extraction of Latex Proteins

Latex proteins were extracted from nonammoniated latex (NAL) harvested from a rubber tree (*Hevea brasiliensis*, clone RRIM600) at the Rubber Research Institute of Malaysia. The NAL was immediately frozen at the site of collection and dispatched to Japan. By thawing and pressing the frozen latex, we obtained a brown liquid that oozed out from it. The liquid (about 100 ml) was supplemented with two tablets of protease inhibitor cocktail (Complete Mini, Roche Applied Science) and dialyzed against running water using Spectra/Por 3 membrane tubing (cutoff 3.5 kD; Spectrum Laboratories, Inc.) overnight. The dialyzate was then lyophilized and reconstituted in phosphate-buffered saline (pH 7.4). After condensation of the solution using Centriprep-10 (cutoff 10 kD; Millipore Co.), the concentrate was ultracentrifuged at 40,000 rpm for 24 h at 4°C (P70AT2 rotor and CP 65β ultracentrifuge, Hitachi Koki Co., Ltd.). The protein content of the supernatant was determined with a BCA Protein Assay Kit (Pierce Chemical Co.) as 13.9 mg/ml. This supernatant was submitted to later study.

Two-Dimensional Gel Electrophoresis

Latex proteins (250 μg) extracted from NAL were diluted in 250 μl of Destreak Rehydration Solution (Amersham Biosciences) supplemented with IPG buffer (0.1%, pH 3–10, nonlinear; Amersham). This solution was used for overnight rehydration of an immobilized pH gradient gel strip (Immobiline DryStrip, Amersham; pH 3–10, nonlinear, 13 cm). Then the strip was submitted to isoelectric focusing on a Multiphor II Electrophoresis Unit (Amersham) at

Table 1. Summary of latex-allergic patients who provided their blood for IgE immunoblotting

Patient No.	Age years	Gender	Occupation	Total IgE IU/ml[1]	Latex-specific IgE IU/ml (score)[2]	Latex SPT	Positive SPT	Other allergic symptoms
1	26	F	nurse	49.1	14.0 (3)	4+	Japanese horseradish	OAS to Japanese horseradish
2	34	F	housewife	1,110	4.50 (3)	4+	avocado, grapefruit	atopic dermatitis, bronchial asthma
3	22	F	dental hygienist	273	2.23 (2)	3+	tomato, spices	OAS, atopic dermatitis, pollinosis
4	25	M	medical doctor	15,500	82.0 (5)	3+	avocado	atopic dermatitis, atopic rhinitis
5	25	F	nurse	88.7	2.81 (2)	3+	–	OAS to melon
6	28	F	nurse	206	15.0 (3)	4+	–	OAS, atopic dermatitis, atopic rhinitis

OAS = Oral allergy syndrome.
1 IgE radioimmunosorbent test (Pharmacia).
2 CAP radioallergosorbent test (Pharmacia).

20 °C. Proteins were focused by applying programmed voltage as follows: 0–300 V in 1 min, 300–3,500 V in 1.5 h and 3,500 V for 7 h. Thereafter, the gel strip was submitted to sodium dodecyl sulfate-polyacrylamide gel electrophoresis (SDS-PAGE) as the second dimension of electrophoresis. Before applying to SDS-PAGE, the gel strip was incubated at room temperature in 7.5 ml of equilibration buffer (Amersham) supplemented by dithiothreitol (1%) for 30 min, then in the same equilibration buffer containing iodoacetamide (1%) instead of dithiothreitol for 30 min. The gel strip was placed on top of a slab gel (10% acrylamide, 14 × 14 cm) and fixed with agarose (0.5%). The second electrophoresis was carried out by applying a constant current of 30 mA for 30 min then 70 mA for 5 h at 20 °C using an SE 600 Ruby Electrophoresis Unit (Amersham).

Immunoblotting

Two-dimensionally separated proteins were transferred onto a polyvinylidene fluoride membrane (14 × 14 cm; Immobilon-P, Millipore) using a semidry transfer cassette (ATTO Co.) by applying a constant current of 200 mA for 1.5 h. SDS (0.1%) was added to each of the discontinuous blotting buffers containing methanol (10%) for efficient transfer of proteins with high molecular weight or a basic isoelectric point. After washing with Tris-buffered saline (TBS; pH 7.4) supplemented with Tween-20 (TBS-T; 0.1%), the membrane was soaked in a chilled and degassed 10 m*M* $NaIO_4$-50 m*M* acetate buffer (pH 4.7) and incubated at 4 °C in the dark overnight. Then the membrane was repeatedly washed with TBS-T and incubated at room temperature in a blocking buffer (Block Ace, Dai-Nippon Pharmaceutical Co.) for 5 h. Following washing with TBS-T, the membrane was incubated overnight in the pooled patients' serum (20 ml) diluted 1/20 in TBS-T at room temperature. In the control experiment, the membrane was incubated in the pooled control serum (20 ml) diluted 1/20 in TBS-T. The next day, the membrane was washed again with TBS-T and incubated at room temperature in a solution of peroxidase-labeled affinity-purified antibodies to human IgE(ε) (Kirkegaard & Perry Laboratories, Inc.) diluted 1/10,000 in TBS-T for 1 h. After repeated washing with TBS-T, IgE-recognized protein spots were visualized using an ECL Western Blotting Detection System and Hyperfilm ECL (Amersham).

In-Gel Digestion

Two-dimensionally separated proteins on the gel were visualized by negative staining [14] using a Zinc Stain Kit (Bio-Rad Laboratories). Protein spots that were judged as IgE-interactive from the immunoblotting with pooled patients' serum were cut out from the gel (highlighted spots in fig. 1A). After treatment with Zinc Destain Solution (Bio-Rad) as instructed by the manufacturer's protocol, the protein spots were submitted to tryptic digestion using a Montage In-Gel Digest96 Kit (Millipore). Digestion proceeded at 30 °C overnight following the manufacturer's recommendations except that *n*-octyl-β-*D*-glucoside (Dojindo Laboratories) was added to the digestion mixture (final 0.1%) for efficient recovery of the fragmented peptides [15].

Mass Spectrometry and Database Search

Fragmented peptides were desalted by means of a reversed-phase microcolumn (ZipTip μC_{18}, Millipore) as instructed by the manufacturer, and eluted from the column with the help of α-cyano-4-hydroxy cinnamic acid solution on a sample plate for mass spectrometry. Matrix-assisted laser desorption/ionization time-of-flight mass spectrometry (MALDI-TOFMS) was performed on a 4700 Proteomics Analyzer (Applied Biosystems Inc.). Positive-ion mass spectra of tryptic peptides were recorded on the reflectron mode of the instrument. The information from these spectra (peptide mass maps, fig. 2A) was used for a database search of the original proteins with the peptide mass fingerprinting (PMF) mode of a search engine (Mascot, Matrix Science). Further, tandem mass spectra (MS/MS spectra) of prominent peptide ions on the peptide mass map were recorded on the time-of-flight (TOF)-TOF mode of the instrument [16]. The information (peptide sequence tag; PST) from such tandem mass spectra (fig. 2B) was employed for a database search with the MS/MS Ion Search mode of Mascot for more precise identification of IgE-interactive proteins. National Center for Biotechnology Information (nonredundant) (NCBInr) was selected as the first database to be searched using Mascot. When there was no candidate with enough certainty, SwissProt and Expressed Sequence Tags (EST) *(H. brasiliensis)* were employed as the second and third databases to be searched, respectively. The taxonomy of the database category was set to *Viridiplantae* (Green Plants), and carbamidomethyl cysteine was selected as a fixed modification of fragmented peptides. The number of allowable missed cleavages in tryptic digestion was set at